PHYSICS AND CHEMISTRY OF SOLID STATE
V. 27, No. 1 (2026) pp. 215-225
Section: Physics

DOI: 10.15330/pcss.27.1.215-225

Vasyl Stefanyk Carpathian National University

ФІЗИКА І ХІМІЯ ТВЕРДОГО ТІЛА
Т. 27, № 1 (2026) С. 215-225
Фізико-математичні науки

PACS: 75.75.-c, 81.07.Bc, 82.50.Hp

ISSN 1729-4428 (Print)
ISSN 2309-8589 (Online)

M. Mokliak[1], R. Ilnytskyi[1], L. Kaykan[2], Yu. Mazurenko[2,3], L. Turovska[4], M. Moiseienko[3], V. Mokliak[2,5], V. Sheketa[6]

Neodymium Doped Copper Ferrite Nanocomposites as an Effective Magnetic Catalyst for the Organic Dyes Decomposition

[1]*Department of Applied Physics and Materials Science, Vasyl Stefanyk Carpathian National University, Ivano-Frankivsk, Ukraine; mariamoklyak@gmail.com*
[2]*Laboratory for Physics of Magnetic Films, G.V. Kurdyumov Institute for Metal Physics, N.A.S. of Ukraine, Kyiv, Ukraine; kaykan@nas.gov.ua, mazurenkoyus@nas.gov.ua, Mokliak_Volodymyr@nas.gov.ua*
[3]*Department of Medical Informatics, Medical and Biological Physics, Ivano-Frankivsk National Medical University, Ivano-Frankivsk, Ukraine; mmoiseyenko@ifnmu.edu.ua*
[4]*Department of Management and Business Administration, Faculty of Management, Vasyl Stefanyk Carpathian National University, Ivano-Frankivsk, Ukraine; liliia.turovska@cnu.edu.ua*
[5]*Department of Physical and Mathematical Sciences, Ivano-Frankivsk National Technical University of Oil and Gas, Ivano-Frankivsk, Ukraine; volodymyr.mokliak@nung.edu.ua*
[6]*Department of Software Engineering, Ivano-Frankivsk National Technical University of Oil and Gas, Ivano-Frankivsk, Ukraine; vasyl.sheketa@nung.edu.ua*

Neodymium-substituted copper ferrite nanoparticles with composition $CuNd_xFe_{2-x}O_4$ (x = 0.00–0.11) were synthesized via the sol–gel autocombustion method and systematically analyzed for their structural, optical, and photocatalytic properties. X-ray diffraction combined with Rietveld refinement confirmed the formation of a dominant spinel ferrite phase with minor secondary phases, while Nd incorporation induced a reduction in crystallite size and an increase in lattice microstrain without disrupting the long-range spinel structure. Optical studies based on diffuse reflectance UV–Vis spectroscopy and Tauc analysis revealed direct allowed electronic transitions and a non-monotonic variation of the optical band gap (2.7–3.1 eV) as a function of Nd content, attributed to the combined effects of lattice distortion, defect states, and cation redistribution. Photocatalytic performance was evaluated through Congo Red degradation under light irradiation in the presence of H_2O_2. Nd substitution significantly enhanced photocatalytic activity, with $CuNd_{0.09}Fe_{1.91}O_4$ showing the highest degradation efficiency (~96%), whereas the highest apparent rate constant (Langmuir–Hinshelwood model) was observed for $CuNd_{0.05}Fe_{1.95}O_4$. The results demonstrate that controlled Nd substitution effectively tunes the structural and electronic properties of $CuFe_2O_4$, leading to improved photocatalytic performance and highlighting its potential for wastewater treatment applications.

Keywords: Spinel ferrites; Copper ferrite nanoparticles; Neodymium substitution; Nanocomposites; Water purification; Photocatalysis.

Received 24 September 2026; Accepted 18 March 2026; Published 30 March 2026.

Introduction

The increasing discharge of organic dyes from textile, paper, leather, and chemical industries poses a serious threat to aquatic ecosystems and human health due to their high toxicity [1], chemical stability, and resistance to conventional wastewater treatment processes [2 – 4]. Azo dyes, such as Congo Red [5], are particularly problematic because of their complex aromatic structure and persistence in the environment. In this context, the development of efficient, low-cost, and recyclable photocatalysts for dye degradation has attracted considerable attention.

Spinel ferrites with the general formula MFe_2O_4

(M = divalent metal ion) have emerged as promising multifunctional materials owing to their chemical stability [6], tunable electronic structure [7], and magnetic properties, which enable facile separation and reuse [8]. Among them, copper ferrite ($CuFe_2O_4$) is of special interest due to its narrow band gap, visible-light absorption capability, and redox-active Cu and Fe cations [9, 10]. However, the photocatalytic efficiency of pristine $CuFe_2O_4$ is often limited by rapid electron–hole recombination and suboptimal charge carrier mobility, necessitating strategies to improve its performance.

Elemental substitution represents an effective approach to tailoring the structural electronic, and magnetic properties of spinel ferrites [7]. In particular, rare-earth ion substitution has been shown to significantly influence crystallite size, lattice strain, cation distribution, and defect density, thereby modifying optical absorption and charge carrier dynamics [11, 12]. Neodymium (Nd^{3+}), characterized by a large ionic radius and strong electronic polarization, can introduce localized lattice distortion and defect states when incorporated into the ferrite lattice [12]. These effects may enhance visible-light absorption, promote charge separation, and improve photocatalytic activity. Despite several reports on rare-earth-doped ferrites, systematic studies correlating Nd substitution, structural distortion, optical band structure, and photocatalytic performance in $CuFe_2O_4$ remain limited.

One way to improve photocatalytic activity is also the use of composite materials [13], which allows for effective modification of their electronic structure and band gap to change the behavior of optical absorption and charge carrier dynamics. In particular, the use of superparamagnetic catalytically active nanocomposites [14, 15] that are easily removed from the reaction medium under the influence of an external magnetic field. Furthermore, combining ferrite photocatalysts with hydrogen peroxide (H_2O_2) activate additional reactive oxygen species via photo-assisted Fenton-like processes, significantly enhancing degradation efficiency [16]. In such systems, the interaction between catalyst structure, electronic properties, and reaction kinetics plays a critical role in determining overall photocatalytic performance. Understanding these structure–property–activity relationships is essential for rational catalyst design.

In this work, Nd-substituted copper ferrite nanoparticles with composition $CuNd_xFe_{2-x}O_4$ (x = 0.00–0.11) were synthesized using the sol–gel autocombustion method [12]. The effects of Nd incorporation on phase composition, crystallite size, lattice strain, and microstructure were systematically investigated using X-ray diffraction and electron microscopy. Optical properties were examined through diffuse reflectance UV–Vis spectroscopy, Tauc analysis, and differential optical methods to elucidate band gap evolution and defect-related absorption features [8, 16]. The photocatalytic activity of the synthesized ferrites was evaluated by Congo Red degradation under light irradiation in the presence of H_2O_2, and the reaction kinetics were analyzed using the Langmuir–Hinshelwood model [8]. The study aims to establish clear correlations between Nd-induced structural and electronic modifications and the resulting photocatalytic performance, providing insights into the design of efficient ferrite-based photocatalysts for wastewater treatment applications.

I. Materials and Methods

1.1. Synthesis of Nd-Substituted Copper Ferrite Nanoparticles

Nd-substituted copper ferrite nanoparticles with nominal composition $CuNd_xFe_{2-x}O_4$ (x = 0.00–0.11) were synthesized using the sol–gel autocombustion method [17]. Analytical-grade iron(III) nitrate nonahydrate ($Fe(NO_3)_3 \cdot 9H_2O$), copper(II) nitrate trihydrate ($Cu(NO_3)_2 \cdot 3H_2O$), neodymium(III) nitrate hexahydrate ($Nd(NO_3)_3 \cdot 6H_2O$), and citric acid monohydrate ($C_6H_8O_7 \cdot H_2O$) were used as starting materials without further purification.

Stoichiometric amounts of the metal nitrates corresponding to the desired $CuNd_xFe_{2-x}O_4$ compositions were dissolved separately in deionized water and then mixed under continuous magnetic stirring to obtain a homogeneous solution. Citric acid was added as a complexing agent and fuel, with the molar ratio of total metal cations to citric acid maintained at unity. The pH of the resulting solution was adjusted to approximately 7 by dropwise addition of a 25% aqueous ammonia solution, promoting effective chelation and gel formation [12].

The mixed solution was heated at moderate temperature under constant stirring until a viscous gel was formed. Further heating led to spontaneous autocombustion, yielding a voluminous, fine powder. The samples were labeled as F0 (x = 0.00) and N1, N3, N5, N7, N9, N11 corresponding to x = 0.01, 0.03, 0.05, 0.07, 0.09, and 0.11, respectively. The obtained powders were subsequently used for structural, microstructural, and optical characterization.

1.2. Structural and Microstructural Characterization

Phase composition and crystal structure of the samples were examined by powder X-ray diffraction using an Empyrean diffractometer (Malvern Panalytical, UK) configured in the Bragg–Brentano reflection mode and employing Cu Kα radiation with a wavelength of 1.5406 Å. XRD data were collected over the angular range of $2\theta = 20°–90°$ using a step increment of 0.033°.

The morphology and chemical composition of the powder samples were examined using scanning electron microscopy (SEM) with a Tescan Vega-3 LMU microscope (TESCAN Brno, s.r.o., Czech Republic) equipped with a Bruker Nano XFlash 410M energy-dispersive X-ray spectrometry (EDX) detector.

For SEM observations, the powder samples were mounted on aluminum stubs using double-sided conductive carbon tape. The measurements were performed in high-vacuum mode (≤ 0.018 Pa) using a motorized stage at an accelerating voltage of 15 keV.

EDX analysis was carried out on selected representative areas of the samples with lateral dimensions on the order of several micrometers, corresponding to the SEM observation regions, at a magnification of approximately 5000× and an accelerating voltage of 15 keV. This approach ensured averaging over multiple

particles and minimized the influence of local compositional fluctuations.

Data acquisition and processing were performed using the ESPRIT 1.9 software package (Bruker Nano GmbH, Berlin, Germany).

1.3. Optical and Photocatalytic Studies

Optical absorption measurements were carried out using a UV/VIS SPECORD 210 PLUS double-beam UV–Vis spectrophotometer (Analytik Jena AG, Germany), operating in the wavelength range from 185 to 1200 nm. The double-beam configuration enabled simultaneous acquisition of sample and reference signals, ensuring high measurement stability and accurate baseline correction. Instrument control, data acquisition, and processing were performed using ASpect UV software with the 21 CFR Part 11 Compliance module (Analytik Jena AG, Germany).

Photocatalytic degradation experiments were performed using $CuNd_xFe_{2-x}O_4$ nanoparticles as the catalyst in the presence of hydrogen peroxide. The catalyst loading was fixed at 0.5 g L^{-1} for all experiments. Hydrogen peroxide (H_2O_2) was added to the reaction mixture at a concentration of 250 mmol L^{-1} to promote the generation of reactive oxygen species.

Congo Red (CR) was used as the model organic dye. The working dye concentration was 10 mg L^{-1} for all $CuNd_xFe_{2-x}O_4$–CR systems. All photocatalytic tests were carried out under identical conditions to ensure reliable comparison of degradation efficiency across different Nd-substituted samples.

II. Results and discussion

2.1. Structural and Morphological Studies

Figure 1(a) displays the X-ray diffraction (XRD) patterns of the synthesized $CuNd_xFe_{2-x}O_4$ nanoparticle series. All compositions exhibit well-defined diffraction peaks that can be indexed to a cubic spinel structure with space group Fd3m [18].

Figure 1 demonstrates that all $CuNd_xFe_{2-x}O_4$ samples are dominated by a spinel-type diffraction pattern, where the main reflections indexed as (111), (220), (311), (400), (422), (511), and (440) are well reproduced by the Rietveld fits (Ycalc) and the difference curves (Yobs−Ycalc) remain close to the baseline, indicating an overall reliable description of the diffraction profiles across the series. The refinement indicates that the primary crystalline phase is the $CuFe_2O_4$ spinel, while minor secondary phases ($CuFeO_2$ and CuO) are also present.

Quantitatively (Table 1), the spinel fraction increases from 81.81% ($CuFe_2O_4$) to ~85–87% at low Nd contents (x = 0.01–0.05), suggesting improved formation of the ferrite phase, whereas at higher substitution levels the spinel fraction slightly decreases to ~86.56–86.57% (x = 0.09–0.11), which may reflect a solubility limit and strain-driven segregation into CuO and $CuFeO_2$ [19]. In parallel, the lattice parameter a varies only slightly (8.3784–8.3820 Å) with a small expansion at intermediate x (x = 0.03–0.07), consistent with Nd-related local lattice distortion without large peak shifts at these low substitution levels. The microstructural parameters evolve more strongly: the crystallite size decreases from 37.6 nm to ~25–31 nm (minimum at x = 0.09, ~25.26 nm), while the microstrain increases from 0.003151 to ~0.00399–0.003996 and then saturates, indicating enhanced lattice defect density and suppressed crystallite growth in the Nd-substituted samples.

The preserved spinel peak set together with modest changes in a but pronounced changes in size and strain supports the conclusion that Nd addition primarily affects the structure through microstructural disorder and local distortions while retaining the long-range spinel framework. These trends provide a structural basis for the optical behavior, since increased strain/disorder and reduced crystallite size modify the absorption edge and contribute to the non-monotonic Eg(x) dependence [20].

Figure 2 shows FESEM images of $CuNd_xFe_{2-x}O_4$ samples (x = 0.00, 0.03, 0.07, and 0.11), revealing an agglomerated microstructure composed of irregularly shaped particles for all compositions. Such agglomeration, typical for chemically synthesized ferrites, arises from magnetic dipole–dipole interactions and partial sintering during combustion [21]. The undoped $CuFe_2O_4$ sample consists of relatively larger agglomerates with plate-like and fractured features, while Nd-substituted samples exhibit more fragmented aggregates composed of finer structural units, indicating suppression of crystallite growth. This trend is consistent with XRD results showing reduced crystallite size and increased microstrain upon Nd incorporation. At the highest Nd content (x = 0.11), the microstructure remains highly agglomerated but becomes more compact, which may be related to increased defect density and partial formation of secondary phases. FESEM observations confirm that Nd substitution primarily induces nanoscale structural refinement within agglomerated particles, supporting the structure–property relationships discussed in the optical analysis section.

2.2. Optical Studies

In spinel ferrites, the optical band gap is determined by electronic transitions involving O 2p states in the valence band and transition-metal 3d states [22] in the conduction band, and is highly sensitive to cation substitution, lattice strain, and nanoscale structural disorder. In $CuNd_xFe_{2-x}O_4$ ferrites, partial replacement of Fe^{3+} by Nd^{3+} introduces local lattice distortion due to the large ionic radius of Nd^{3+}, alters cation distribution within octahedral sites, and modifies the degree of p–d orbital hybridization, all of which directly affect the optical absorption edge [23, 24].

Diffuse reflectance UV–Vis spectroscopy was used to quantify these effects through determination of the optical band gap energy Eg. The absorption behavior was analyzed using the Tauc relation [8],

$$(ahv)^n = A\left(hv - E_g\right),$$

where alpha is the absorption coefficient, hv is the photon energy, A is a proportionality constant, and n depends on the nature of the electronic transition.

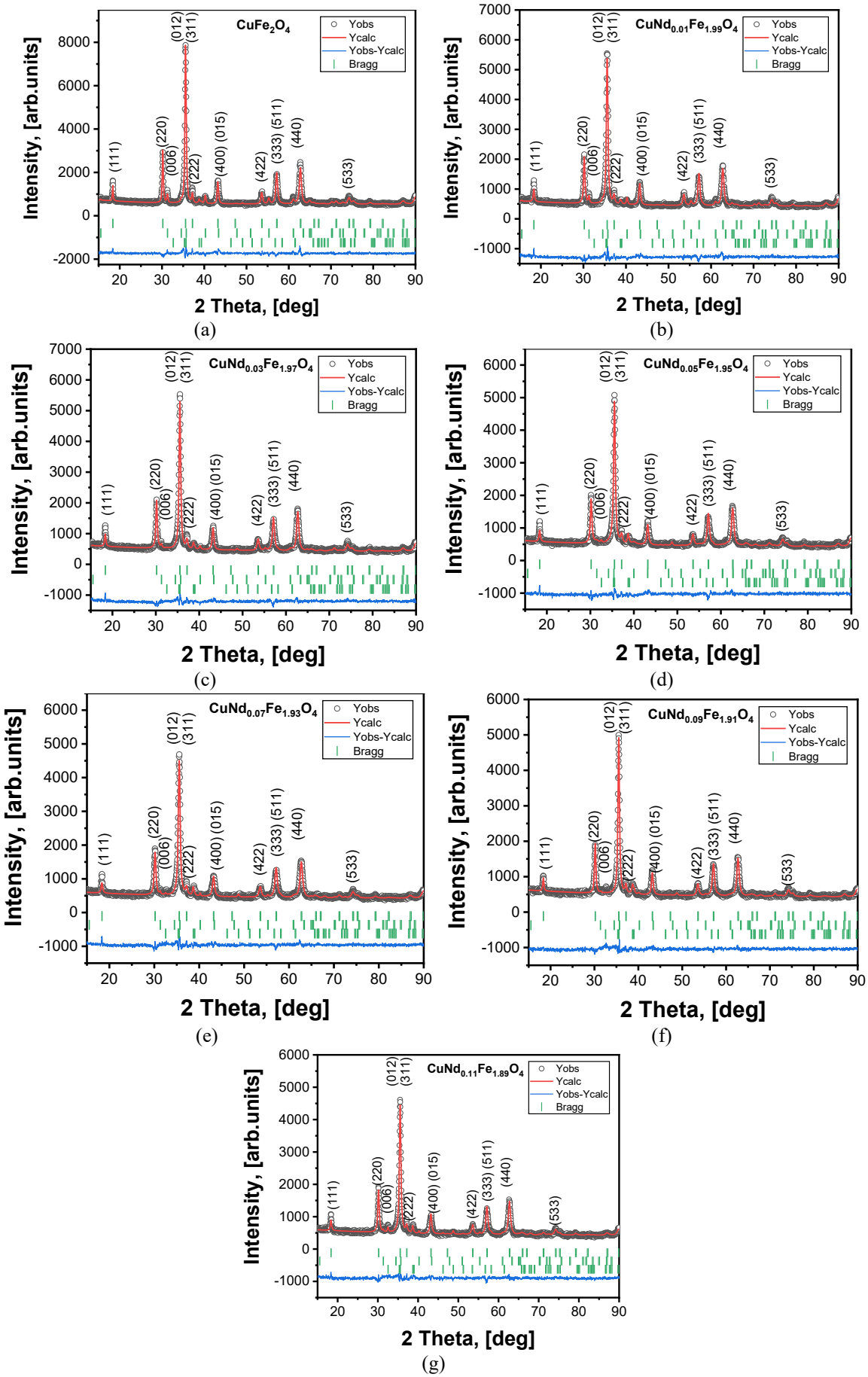

Fig. 1. Rietveld refinement profile of XRD data of as prepared $CuNd_xFe_{2-x}O_4$ samples. The dots correspond to the experimental data and the solid line is for the Rietveld refinement fit. The lower curve is the difference between the observed and calculated at each step.

Table 1.

Phase Composition and Structural Parameters of $CuNd_xFe_{2-x}O_4$ Nanoparticles

Sample	$CuFe_2O_4$			$CuFeO_2$, %	CuO, %	Lattice strain
	Phase, %	a, Å	Crystallite size, nm			
$CuFe_2O_4$	81.81	8.3798	37.6	14.28	3.91	0.00315
$CuNd_{0.01}Fe_{1.99}O_4$	85.54	8.3784	31.53	10.66	3.81	0.00381
$CuNd_{0.03}Fe_{1.97}O_4$	87.49	8.3812	30.45	7.19	5.32	0.00388
$CuNd_{0.05}Fe_{1.95}O_4$	87.47	8.382	27.06	6.67	6.27	0.00396
$CuNd_{0.07}Fe_{1.93}O_4$	86.75	8.382	26.54	6.19	7.05	0.00399
$CuNd_{0.09}Fe_{1.91}O_4$	86.57	8.3805	25.26	5.8	7.63	0.00400
$CuNd_{0.11}Fe_{1.89}O_4$	86.56	8.3799	26.09	6.49	6.94	0.00399

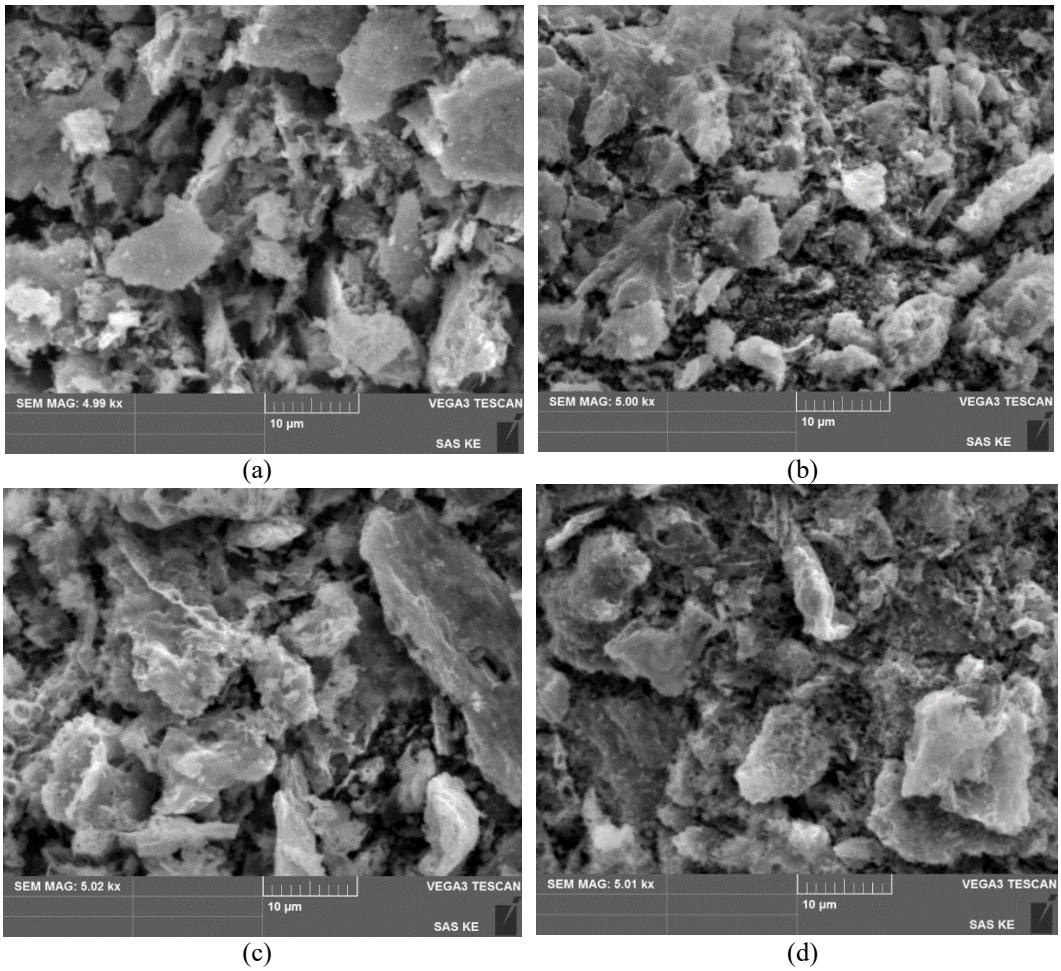

Fig. 2. FESEM images for 0.00 (a), 0.03 (b), 0.07 (c) and 0.11 (d) of $CuNd_xFe_{2-x}O_4$ samples.

Figure 3 shows the Tauc plots for $CuNd_xFe_{2-x}O_4$ ferrites, confirming that the dominant optical absorption edge can be treated as a direct allowed transition for all compositions, and reveals a non-monotonic dependence of the optical band gap Eg on Nd content. The undoped $CuFe_2O_4$ sample exhibits Eg = 2.86 eV, consistent with nanoscale copper ferrites, while low Nd^{3+} substitution (x = 0.01–0.05) leads to a slight band-gap reduction (2.76–2.82 eV) due to defect-related band tailing caused by lattice distortion from the larger Nd^{3+} ionic radius. As summarized in Table 1, low–Nd-substitution compositional range is characterized by a pronounced reduction in crystallite size (from ~37.6 to ~30 nm) and increasing microstrain. At intermediate Nd contents (x ≈ 0.07–0.10), the crystallite size reaches a minimum (~26–27 nm) and microstrain reaches its maximum, accompanied by slight lattice expansion, resulting in a sharp increase of Eg up to ~3.10 eV. This behavior reflects the combined influence of size reduction, enhanced lattice strain, and modified cation distribution, which alters O 2p–Fe 3d hybridization and widens the band gap [25]. At higher Nd concentrations, the emergence of secondary phases (CuO and $CuFeO_2$) and increased structural disorder counteract these effects, leading to a subsequent decrease in Eg.

For comparative purposes across the series, Eg was operationally extracted from the high-energy linear region assuming direct allowed transition; additional sub-band

features observed in differential analysis reflect defect-related states and do not contradict the comparative Eg definition. Figure 4 illustrates the optical absorption behavior of the $CuFe_2O_4$ sample analyzed using both the conventional Tauc method and a differential approach [26, 27]. In Figure 4a, the Tauc plot $(\alpha h\nu)^2$ versus $h\nu$ exhibits several quasi-linear regions rather than a single well-defined absorption edge. Extrapolation of these regions yields apparent transition energies at approximately 1.57 eV, 2.14 eV, and 2.99 eV, suggesting that more than one absorption mechanism contributes to the optical response and that $CuFe_2O_4$ cannot be fully described by a single direct band-to-band transition.

To further resolve these features, Figure 4b shows the first derivative $d(\ln(\alpha h\nu))/d(h\nu)$. Distinct maxima occur at about 1.57 eV, 2.14 eV, 2.35 eV, and 2.65 eV, indicating multiple absorption-related features. The lowest-energy feature (~1.57 eV) may be associated with defect- or disorder-induced localized states typical for nanoscale ferrites, while the features in the 2.1–2.7 eV range can be attributed to additional electronic transitions and defect-assisted absorption involving O 2p and transition-metal 3d

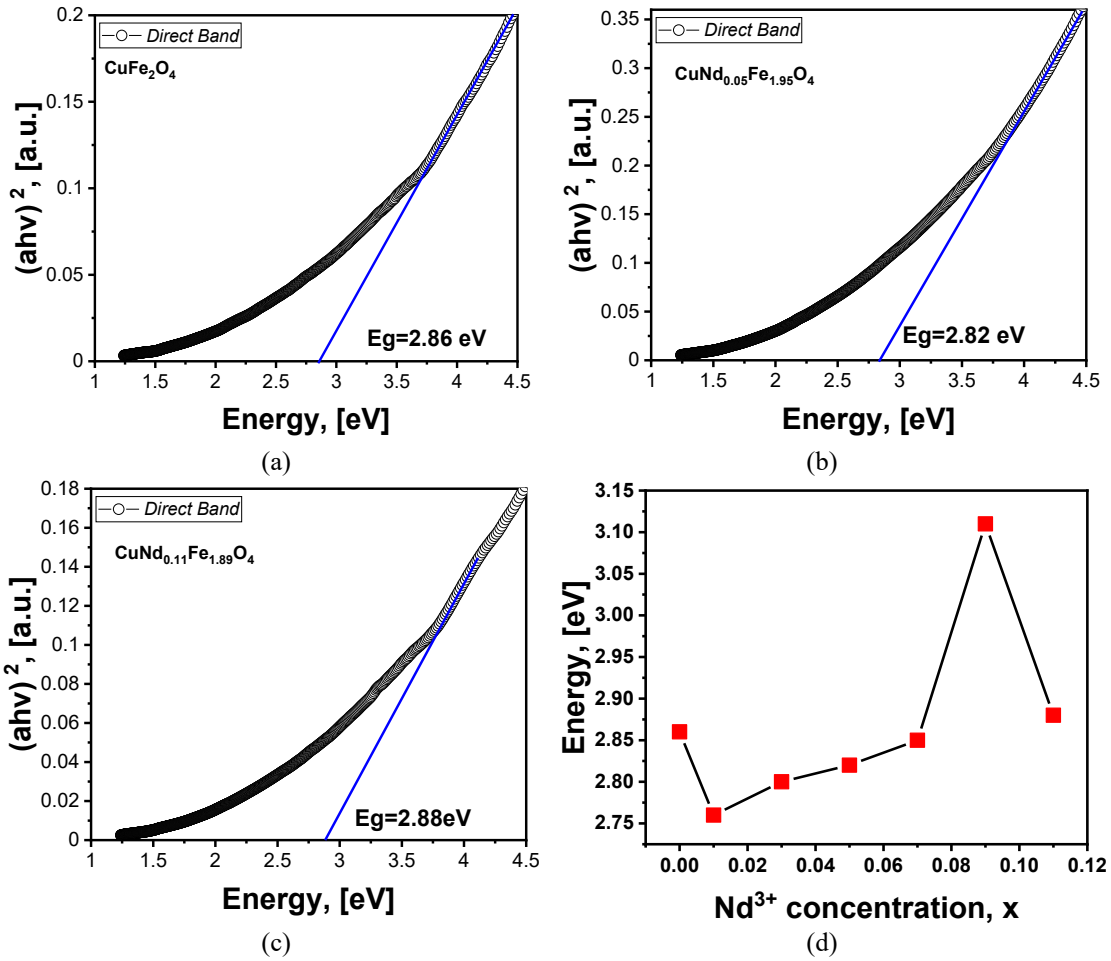

Fig. 3. Tauc plot for determining the optical band gap (Eg) for $CuNd_xFe_{2-x}O_4$ samples with direct allowed transitions.

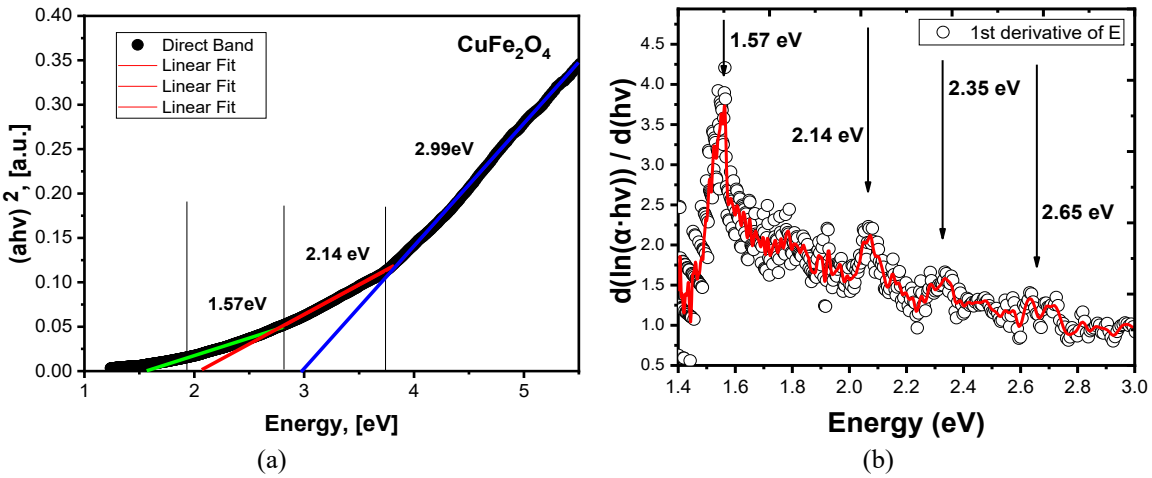

Fig. 4. Differential plot for $CuFe_2O_4$ sample.

states.

The highest-energy transition near ~2.99 eV, extracted from the high-energy linear region of the Tauc plot, represents the apparent high-energy absorption edge, which is slightly higher than the effective Eg extracted in Figure 3 due to the influence of sub-band absorption and band tailing on the Tauc analysis. The coexistence of lower-energy features highlights the influence of defect states, cation disorder, and lattice imperfections on the optical response of ferrite nanoparticles [28].

The combined Tauc and differential analyses indicate a multi-feature absorption behavior where band-edge transitions coexist with sub-band absorption, explaining the broad absorption edge observed in UV–Vis spectra.

2.3. Photocatalytic Studies

Figure 5 presents the time-dependent UV–Vis absorption spectra of Congo Red in the presence of $CuNd_xFe_{2-x}O_4$ photocatalysts under light irradiation. For all samples, the characteristic absorption band of Congo Red in the visible region progressively decreases with irradiation time, indicating continuous degradation of the dye molecules. No noticeable shift in the absorption maximum is observed, suggesting that the degradation proceeds primarily through destruction of the chromophoric structure [29] rather than simple molecular transformation.

The undoped $CuFe_2O_4$ sample (Figure 5a) exhibits a gradual decrease in absorbance, reflecting moderate photocatalytic activity. Upon Nd substitution, a more pronounced reduction in absorption intensity is observed, particularly for $CuNd_{0.03}Fe_{1.97}O_4$ and $CuNd_{0.07}Fe_{1.93}O_4$ (Figure 5b, c), indicating enhanced photocatalytic efficiency. This improvement is consistent with the structural and optical modifications induced by Nd incorporation [30], such as reduced crystallite size, increased lattice strain, and altered electronic structure, which can facilitate charge carrier generation and separation.

Figure 6a compares the photocatalytic performance of pure and Nd-substituted copper ferrites through the normalized concentration ratio C/C_0 as a function of irradiation time. All samples exhibit a continuous decrease in C/C_0 after light exposure, confirming effective photocatalytic degradation of Congo Red. The undoped $CuFe_2O_4$ (F0) shows a moderate degradation rate, reaching a removal efficiency of about 78.2% after 180 min. Nd substitution leads to a clear enhancement in photocatalytic activity, with faster decay of C/C_0 observed for most doped compositions. In particular, samples with intermediate Nd contents (N5 and N9) display the most pronounced degradation behavior, consistent with the stronger absorbance decay observed in Figure 5.

The reaction kinetics were analyzed using a Langmuir-Hinshelwood model [7], as shown in Figure 6b, where linear relationships between $\ln(C_0/C)$ and

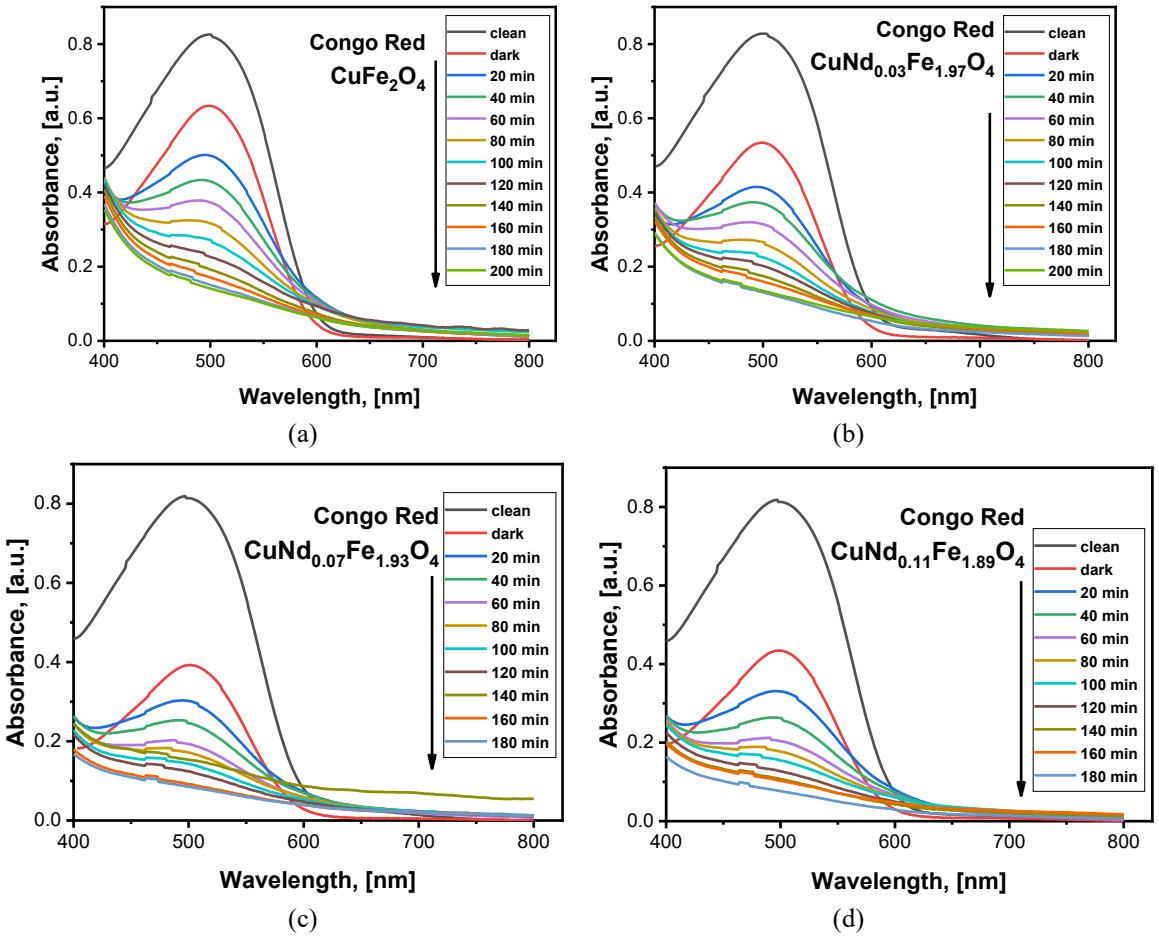

Fig. 5. Time-dependent UV-Vis absorption spectra of (a) $CuFe_2O_4$, (b) $CuNd_{0.03}Fe_{1.97}O_4$, (c) $CuNd_{0.07}Fe_{1.93}O_4$, and (d) $CuNd_{0.11}Fe_{1.89}O_4$ nanoparticles. The decrease in absorbance intensity over time indicates the photocatalytic degradation efficiency of the samples under light irradiation.

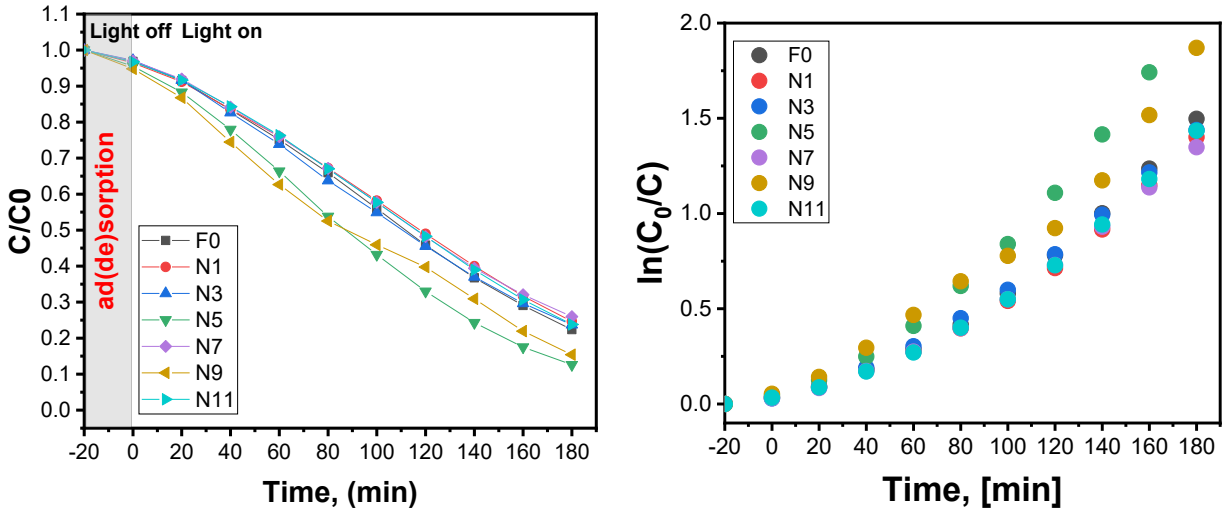

(a) (b)

Fig. 6. Photocatalytic performance and kinetic study of Congo Red degradation: (a) Variation of C/C_0 as a function of irradiation time; (b) Pseudo-first-order kinetic plots of $\ln(C_0/C)$ versus time for the pure (F0) and Neodymium-substituted (N1–N11) copper ferrite samples.

Table 2.

Langmuir–Hinshelwood kinetic parameters for Congo Red photocatalytic degradation over $CuNd_xFe_{2-x}O_4$ samples, where k_{L-H} is the apparent pseudo-first-order rate constant, R^2 is the linear fit coefficient, t is the irradiation time, and K_{max} is the maximum degradation efficiency.

Sample	$K_{L-H} \times 10^{-2}$, min^{-1}	R2	t, min	Kmax, %
$CuFe_2O_4$	0.00932	0.96	180	78.20
$CuNd_{0.01}Fe_{1.99}O_4$	0.00867	0.96	180	80.66
$CuNd_{0.03}Fe_{1.97}O_4$	0.00870	0.96	180	81.28
$CuNd_{0.05}Fe_{1.95}O_4$	0.01260	0.96	180	84.71
$CuNd_{0.07}Fe_{1.93}O_4$	0.00816	0.97	180	88.31
$CuNd_{0.09}Fe_{1.91}O_4$	0.01185	0.97	180	95.93
$CuNd_{0.11}Fe_{1.89}O_4$	0.00906	0.97	180	88.51

irradiation time are obtained for all samples. The high correlation coefficients ($R^2 \approx 0.96$–0.97) listed in Table 2 confirm that the photocatalytic degradation of Congo Red follows pseudo-first-order kinetics over the investigated time range. The apparent rate constants (k_{L-H}) further quantify the effect of Nd substitution. Compared to $CuFe_2O_4$ ($k = 0.00932 \times 10^{-2}$ min^{-1}), a noticeable increase in the rate constant is observed for $CuNd_{0.05}Fe_{1.95}O_4$ (0.01260×10^{-2} min^{-1}) and $CuNd_{0.09}Fe_{1.91}O_4$ (0.01185×10^{-2} min^{-1}), which also show high degradation efficiencies of 84.7% and 95.9%, respectively.

The non-monotonic dependence of both the kinetic constant and maximum degradation efficiency on Nd content reflects the competing effects of structural and electronic modifications induced by Nd incorporation [31]. As discussed in the structural and optical sections, moderate Nd substitution reduces crystallite size, increases lattice strain, and modifies the band structure, which can enhance charge carrier generation and suppress electron–hole recombination. These factors collectively improve photocatalytic efficiency for intermediate Nd concentrations. At higher Nd content (N11), although substantial degradation (≈88.5%) is still achieved, the slight decrease in k_{L-H} suggests that excessive structural disorder and the presence of secondary phases may introduce recombination centers, partially counteracting the beneficial effects.

The results demonstrate that Nd substitution effectively tunes the photocatalytic activity of $CuFe_2O_4$, with $CuNd_{0.09}Fe_{1.91}O_4$ exhibiting the optimal balance between structural disorder and electronic efficiency, leading to the highest Congo Red degradation rate under the studied conditions.

Conclusions

Nd-substituted copper ferrite nanoparticles with composition $CuNd_xFe_{2-x}O_4$ (x = 0.00–0.11) were successfully synthesized via the sol–gel autocombustion method, and their structural, optical, and photocatalytic properties were systematically investigated. X-ray diffraction and Rietveld refinement confirmed the formation of a dominant spinel ferrite phase for all compositions, with minor amounts of CuO and $CuFeO_2$ as secondary phases. Nd incorporation did not disrupt the long-range spinel structure but induced significant microstructural changes, including a pronounced reduction in crystallite size and an increase in lattice microstrain, reaching a maximum at intermediate Nd contents.

Optical studies based on diffuse reflectance UV–Vis

spectroscopy and Tauc analysis revealed direct allowed electronic transitions for all samples and a non-monotonic dependence of the optical band gap on Nd concentration. The band gap varied within the range of approximately 2.7–3.1 eV and was governed by the interaction between crystallite size reduction, lattice strain, defect-related band tailing, and modified O 2p–Fe 3d hybridization. Differential optical analysis further demonstrated that the optical response of $CuFe_2O_4$ consists of multiple absorption contributions, highlighting the role of defect- and disorder-related sub-band states.

Photocatalytic performance was evaluated through the degradation of Congo Red under light irradiation in the presence of H_2O_2. Nd substitution significantly enhanced the photocatalytic activity compared to undoped $CuFe_2O_4$. The degradation process followed the Langmuir–Hinshelwood pseudo-first-order kinetic model with high correlation coefficients. Among the investigated compositions, $CuNd_{0.09}Fe_{1.91}O_4$ exhibited the highest photocatalytic efficiency (~96%), whereas the highest apparent rate constant was observed for $CuNd_{0.05}Fe_{1.95}O_4$. This behavior is attributed to the optimal balance between structural disorder, electronic structure modification, and suppression of charge carrier recombination. At higher Nd contents, excessive disorder and secondary phase formation partially reduced the photocatalytic performance.

The results demonstrate that controlled Nd substitution is an effective strategy for tuning the structure and electronic properties of $CuFe_2O_4$, leading to substantially improved photocatalytic efficiency. These findings highlight the potential of Nd-substituted copper ferrites as efficient and magnetically recoverable photocatalysts for the degradation of organic pollutants in wastewater treatment applications.

Data Availability Statement:
Data is contained within the article.

Acknowledgments:
The authors are grateful to the Academic Centre for Materials and Nanotechnology AGH University of Krakow, Krakow, Poland for VSM measurements. Authors are grateful to the Department of Solid State Physics, AGH University of Krakow, Krakow, Poland for XRD measurements.

Mokliak Mariia – PhD Student, Department of Applied Physics and Materials Science;
Kaykan Larysa – Doctor of Physical and Mathematical Sciences, Senior Researcher, Leading Research Scientist at the Laboratory for Physics of Magnetic Films;
Mazurenko Yuliia – Candidate of Physical and Mathematical Sciences (Ph.D.), Research Scientist at Laboratory for Physics of Magnetic Films;
Turovska Liliia – Candidate of Chemical Sciences (Ph.D), Vice-Rector for Research and International Affairs;
Moiseienko Mykola – Doctor of Biological Sciences, Professor, Head of the Department of Medical Informatics, Medical and Biological Physics;
Mokliak Volodymyr – Doctor of Physical and Mathematical Sciences, Professor of the Department of Physical and Mathematical Sciences, Head of Laboratory for Physics of Magnetic Films;
Sheketa Vasyl – Doctor of Technical Sciences, Professor, Professor of the Department of Software Engineering.

[1] M.F. Shahriar, T. Kamal, R. Rahman, *Durability challenges of concrete structures in chemically aggressive riverine zones contaminated by textile discharge: a brief review*, Discover Civil Engineering, 2(1), 1 (2025); https://doi.org/10.1007/s44290-025-00349-y.
[2] A.L.T. Zheng, K.S. Rajoo, C.M. Manivel, E.Y.L. Teo, O.F. Marzuki, S. Boonyuen, E.L.T. Chung, Y. Andou, , *Leather waste into functional materials: composite nanoarchitectonics, energy systems, and environmental applications*, International Journal of Energy and Water Resources 10(1), 1 (2025); https://doi.org/10.1007/s42108-025-00433-0.
[3] N.Ya. Ivanichok, I.M. Budzuliak, M.I. Moiseienko, R.P. Lisovskiy, B.I. Rachii, A.M. Gamarnyk, L.V. Turovska, S.A. Lisovska, *Electrochemical properties of nanoporous carbon materials obtained from raw materials of plant origin (hemp shives)*, Physics and Chemistry of Solid State, 21(1), 35 (2020); https://doi.org/10.15330/pcss.21.1.35-42.
[4] V. Moklyak, A. Hrubiak, Z. Gogitidze, Y. Yavorskyi, *Biopolimer Peptide Batteries – A New Concept for Environmentally Friendly and Safer Energy Storage*, Batteries, 7(3), 50(2021); https://doi.org/10.3390/batteries7030050.
[5] N.P. Raval, P.U. Shah, N.K. Shah, *Adsorptive amputation of hazardous azo dye Congo red from wastewater: a critical review,* Environmental Science and Pollution Research, 23(15), 14810(2016); https://doi.org/10.1007/s11356-016-6970-0.
[6] E.A. Schultz-Sikma, H.M. Joshi, Q. Ma, K. W. MacRenaris, A. L. Eckermann, V.P. Dravid, T.J. Meade, , *Probing the chemical stability of mixed ferrites: implications for magnetic resonance contrast agent design*, Chemistry of Materials, 23(10), 2657 (2011); https://doi.org/10.1021/cm200509g.
[7] J. Mazurenko, A. K. Sijo, L. Kaykan, Ł. Gondek, J. M. Michalik, L. Matzui, L. Vovchenko, O. Yakovenko, *Optimizing the structural, morphological, and dielectric properties of copper ferrite through magnesium substitution,* Applied Physics A, 131(9), 1 (2025); https://doi.org/10.1007/s00339-025-08741-2.
[8] J. Mazurenko, L. Kaykan, A. K. Sijo, A. Zywczak, M. Marzec, L. Turovska, K. Hreus, *Photocatalytic efficiency of nickel-doped copper ferrite in organic dye decomposition*, Nano-Structures & Nano-Objects, 45, 101603 (2026); https://doi.org/10.1016/j.nanoso.2025.101603.

[9] K. Derkaoui, A. Elfiad, Y. Mebdoua, I. Belkhettab, I. Bencherifa, S. Benredouane, S. Naama, T. Hadjersi, M. Kechouane, Reaction Kinetics, *Optical and dielectric properties of $CuFe_2O_4$ nanoparticles: a pathway to efficient photocatalytic degradation of Rhodamine B under visible light*, Mechanisms and Catalysis, 138(5), 3521 (2025); https://doi.org/10.1007/s11144-025-02906-z.

[10] Q. Sun, X. Wang, Y. Liu, S. Xia, J. Zhao, *Activation of peroxymonosulfate by a floating oxygen vacancies–$CuFe_2O_4$ photocatalyst under visible light for efficient degradation of sulfamethazine,* Science of the Total Environment, 824, 153630 (2022); https://doi.org/10.1016/j.scitotenv.2022.153630.

[11] A. Kiran, M. N. Akhtar, M. Yousaf, K. M. Batoo, O. M. Aldossary, S. N. Khan, *Influence of Y3+, Yb3+, Gd3+ cations on structural and electromagnetic properties of CuFe2O4 nanoferrites prepared via one-step sol–gel method*, Journal of Rare Earths, 39 (10), 1224 (2021); https://doi.org/10.1016/j.jre.2020.12.003.

[12] M. Mokliak, L. Kaykan, J. Mazurenko, M. Moiseienko, M. Kuzyshyn, I. Dovbnia, N. Ilnitsky, S. Yuryev, V. Mokliak, *Influence of neodymium doping on the thermomagnetic response and colloidal behavior of copper ferrite nanoparticles*, Physics and Chemistry of Solid State, 26(3), 564(2025); https://doi.org/10.15330/pcss.26.3.564-577.

[13] V. Moklyak, V. Chelyadyn, A. Hrubiak, B. Ostafiychuk, V. Kotsyubynsky, M. Mizilevska, M. Moklyak, R. Lisovskyy, Y. Yavorskyi, *Synthesis, Structure, Optic and Photocatalytic Properties of Anatase/Brookite Nanocomposites*, Journal of Nano Research, 64, 39 (2020); https://doi.org/10.4028/www.scientific.net/jnanor.64.39.

[14] V.O. Kotsyubynsky, V.V. Mokliak, A.B. Grubiak, P.I. Kolkovsky, A.S.A.H. Zamil, *Nanocomposite Materials alfa-Fe_2O_3/gamma-Fe_2O_3: Synthesis, Crystal and Magnetic Microstructure, Morphology*, Journal of Nano- and Electronic Physics, 5(1), 1024-1 (2013).

[15] V. O. Kotsyubynsky, A. B. Grubiak, V. V. Moklyak, V. M. Pylypiv, R. P. Lisovsky, *Noveishie Tekhnol., Structural, Morphological, and Magnetic Properties of the Mesoporous Maghemite Synthesized by a Citrate Method*, Metallofiz, 36(11), 1497 (2014); https://doi.org/10.15407/mfint.36.11.1497.

[16] J. Mazurenko, L. Kaykan, V. Moklyak, M. Petryshyn, O. Mazurenko, S. Leleko, *Photocatalytic degradation of methylene blue in aqueous media using magnesium-substituted copper ferrite as a magnetic catalyst,* Physics and Chemistry of Solid State, 25(3), 605 (2024); https://doi.org/10.15330/pcss.25.3.605-616.

[17] J. Mazurenko, L. Kaykan, V. Moklyak, M. Moklyak, M. Moiseienko, N. Ostapovych, M. Petryshyn, *Inductive heating behavior of copper ferrite magnetic nanoparticles*, Physics and Chemistry of Solid State, 26(2), 312 (2025); https://doi.org/10.15330/pcss.26.2.312-321.

[18] V.N. Nikolić, M.M. Vasić, D. Kisić, *Observation of c-CuFe2O4 nanoparticles of the same crystallite size in different nanocomposite materials: the influence of Fe^{3+} cations*, Journal of Solid State Chemistry, 275, 187 (2019); https://doi.org/10.1016/j.jssc.2019.04.007.

[19] S. Bilgin, Ü. Alver, *A comparative study of structural, magnetic, and thermal properties of $CuxFe_{3-x}O_4$ nanoparticles prepared in open and closed systems using solution combustion synthesis*, Journal of Sol-Gel Science and Technology, 107(3), 810 (2023); https://doi.org/10.1007/s10971-023-06170-2.

[20] M.N. Nawaz, U. Ghazanfar, W. Yuan, H. Wahab, O.T. Satti, S. B. Khan, *Materials in Electronics, Impact of cobalt doping on the properties of zinc ferrite ($CoxZn_{1-x}Fe_2O_4$),* Journal of Materials Science, 36(13), 1 (2025); https://doi.org/10.1007/s10854-025-14770-7.

[21] L. Gama, E. P. Hernandez, D. R. Cornejo, A. A. Costa, S. M. Rezende, R. H. G. A. Kiminami, A. C. F. M. Costa, *Magnetic and structural properties of nanosize Ni–Zn–Cr ferrite particles synthesized by combustion reaction,* Journal of Magnetism and Magnetic Materials, 317(1–2), 29 (2007); https://doi.org/10.1016/j.jmmm.2007.04.007.

[22] M.A. Rafiq, A. Javed, M.N. Rasul, M.A. Khan, A. Hussain, *Understanding the structural, electronic, magnetic and optical properties of spinel MFe2O4 (M = Mn, Co, Ni) ferrites*, Ceramics International, 46(4), 4976 (2020); https://doi.org/10.1016/j.ceramint.2019.10.237.

[23] S. Caliskan, A.M. Rodriguez, S. Alexander, M.A. Almessiere, A. Baykal, Y. Slimani, *Electronic, magnetic and optical properties of CoNi spinel ferrites doped by rare earth atoms: a density functional theory study*, Discover Materials, 4(1), 1 (2024); https://doi.org/10.1007/s43939-024-00093-7.

[24] M. Naveed-Ul-Haq, S. Hussain, S. Webers, S. Salamon, I. Ahmad, T. Bibi, A. Hameed, H. Wende, *On the structure–property relationships of (Al, Ga, In)-doped spinel cobalt ferrite compounds: a combined experimental and DFT study*, Physical Chemistry Chemical Physics, 23(33), 18112 (2021); https://doi.org/10.1039/d1cp02625a.

[25] D.H. Taffa, R. Dillert, A.C. Ulpe, K.C.L. Bauerfeind, T. Bredow, D.W. Bahnemann, M. Wark, *Photoelectrochemical and theoretical investigations of spinel-type ferrites ($MxFe_{3-x}O_4$) for water splitting: a mini-review*, Journal of Photonics for Energy, 7(1), 012009 (2016); https://doi.org/10.1117/1.jpe.7.012009.

[26] L. C. Xue, L.Q. Wu, S.Q. Li, Z.Z. Li, G.D. Tang, W.H. Qi, X.S. Ge, L.L. Ding, *Study of electron transition energies between anions and cations in spinel ferrites using differential UV–vis absorption spectra*, Physica B: Condensed Matter, 492, 61 (2016); https://doi.org/10.1016/j.physb.2016.04.002.

[27] G.D. Tang, Q.J. Han, J. Xu, D.H. Ji, W.H. Qi, Z.Z. Li, Z.F. Shang, X.Y. Zhang, *Investigation of magnetic ordering and cation distribution in the spinel ferrites $CrxFe_{3-x}O_4$ ($0.0 \le x \le 1.0$),* Physica B: Condensed Matter, 438, 91 (2014); https://doi.org/10.1016/j.physb.2014.01.010.

[28] C. Ravi Dhas, R. Venkatesh, K. Jothivenkatachalam, A. Nithya, B. Suji Benjamin, A. Moses Ezhil Raj, K. Jeyadheepan, C. Sanjeeviraja, *Visible light-driven photocatalytic degradation of Rhodamine B and Direct Red using cobalt oxide nanoparticles*, Ceramics International, 41(8), 9301 (2015); https://doi.org/10.1016/j.ceramint.2015.03.238.

[29] V.S. Kirankumar, B. Hardik, S. Sumathi, *Photocatalytic degradation of Congo red using copper-substituted cobalt ferrite*, IOP Conference Series: Materials Science and Engineering, 263, 022027 (2017); https://doi.org/10.1088/1757-899x/263/2/022027.

[30] M.A. Wahba, R.K. Khaled, *Enhanced optical and photocatalytic features of Gd-doped and Gd/Nd co-doped $CoFe_2O_4$ nanostructures*, Journal of Rare Earths, 1 (2025); https://doi.org/10.1016/j.jre.2025.06.007.

[31] T.T.N. Phan, T.H.N. Chu, *Enhanced degradation of phenol by visible light-assisted Fenton catalytic activity of copper-substituted neodymium ferrite,* Environmental Processes, 10(2), 1 (2023); https://doi.org/10.1007/s40710-023-00639-6.

М. Мокляк[1], Л. Кайкан[2], Ю. Мазуренко[2,3], Л. Туровська[4], М. Мойсеєнко[3], В. Мокляк[2,5], В. Шекета[6]

Нанокомпозити на основі мідного фериту заміщеного неодимом, як ефективний магнітний каталізатор для деградації органічних барвників

[1]*Кафедра прикладної фізики та матеріалознавства, Карпатський національний університет імені Василя Стефаника, Івано-Франківськ, Україна, mariamoklyak@gmail.com*

[2]*Лабораторія фізики магнітних плівок, Інститут металофізики імені Г.В. Курдюмова НАН України, Київ, Україна; kaykan@nas.gov.ua, mazurenkoyus@nas.gov.ua, Mokliak_Volodymyr@nas.gov.ua*

[3]*Кафедра медичної інформатики, медичної та біологічної фізики, Івано-Франківський національний медичний університет, Івано-Франківськ, Україна, mmoiseyenko@ifnmu.edu.ua;*

[4]*Кафедра менеджменту та бізнес-адміністрування, факультет менеджменту, Карпатський національний університет імені Василя Стефаника, Івано-Франківськ, Україна; liliia.turovska@cnu.edu.ua*

[5]*Кафедра фізико-математичних наук, Івано-Франківський національний технічний університет нафти і газу, Івано-Франківськ, Україна; volodymyr.mokliak@nung.edu.ua*

[6]*Кафедра інженерії програмного забезпечення, Івано-Франківський національний технічний університет нафти і газу, Івано-Франківськ, Україна; vasyl.sheketa@nung.edu.ua*

Неодим-заміщені наночастинки мідного фериту складу $CuNd_xFe_{2-x}O_4$ (x = 0.00–0.11) були синтезовані методом золь-гель автогоріння та досліджено їхні структурні, оптичні й фотокаталітичні властивості. Рентгенівська дифракція в поєднанні з уточненням Рітвельда підтвердила утворення домінуючої фази шпінельного фериту з незначними вторинними фазами, тоді як включення Nd викликало зменшення розміру кристалітів та збільшення мікродеформації ґратки без руйнування далекого порядку шпінельної структури. Оптичні дослідження на основі UV–Vis спектроскопії та аналізу Така виявили прямі дозволені електронні переходи й немонотонну зміну ширини оптичної забороненої зони (2.7–3.1 еВ) зі зростанням вмісту Nd, що зумовлено сукупною дією спотворення ґратки, дефектних станів і перерозподілу катіонів. Фотокаталітичну ефективність оцінювали за деградацією барвника Конго червоний під дією світлового опромінення у присутності H_2O_2. Заміщення Nd значно підвищило фотокаталітичну активність, зразок $CuNd_{0.09}Fe_{1.91}O_4$ показав найвищу ефективність деградації (~96%), тоді як найвища видима константа швидкості (модель Ленгмюра-Хіншелвуда) спостерігалася для $CuNd_{0.05}Fe_{1.95}O_4$. Результати показують, що контрольоване заміщення Nd ефективно змінює структурні та електронні властивості $CuFe_2O_4$, що призводить до покращення фотокаталітичної активності та підкреслює його потенціал для застосування в очищенні води.

Ключові слова: шпінельні ферити; наночастинки мідного фериту; заміщення неодимом; нанокомпозити; очищення води; фотокаталіз.